JSAEM Studies in Applied Electromagnetics and Mechanics, 12

SUPERCONDUCTIVITY AND MAGNETIC MATREIALS

Proceedings of
The Second Japanese-Greek Joint Workshop on Superconductivity and Magnetic Materials
May 10-11, 2001, Oita, Japan

Editors:

M. Enokizono
Oita University
Oita, Japan

A.G. Mamalis
National Technical University of Athens
Athens, Greece

Superconductivity and Magnetic Materials
M. Enokizono and A.G. Mamalis (eds.)

Visualization of Magnetization Dynamics

Hisashi Endo, Seiji Hayano, and Yoshifuru Saito
Graduate School of Engineering, HOSEI University,
3-7-2 Kajino, Koganei, 184-8584 Tokyo, Japan

Abstract. This paper proposes a visualizing methodology of iron loss in a magnetic material using its visualized domain images, i.e., SEM, Kerr and Faraday effects. Our image analysis methodology based on classical field theory leads to the image differential equations. A dynamic image, so called animation, is given as a solution of Helmholtz type partial differential equation in particular. The state transition matrix, given in the Helmholtz equation, derived from a series of distinct visualized domain images representing magnetized state makes it possible to visualize the magnetizing mechanism as well as iron loss generation. In the present paper, visualization of iron loss generation is worked out using a set of SEM images representing the domain pattern of a grain-oriented electrical steel sheet by mean of image Helmholtz equation. Based on the state transition matrix derived from three distinct SEM images we have succeeded in visualizing and quantifying the behaviors of magnetic domains, i.e., magnetic boundary displacement, delay of magnetic domain movement, lancet domain generation and so on.

1. Introduction

A lot of magnetic domain observation methodologies are available to clarify the physics of magnetic material behavior [1]. This provides us a visualized image of the magnetic materials. Consideration of magnetic domain behaviors such as domain structure and boundary displacement leads to the evaluation of magnetic materials [2]. In order to accomplish this in a most efficient manner, we have proposed an image processing methodology for evaluating the precise characteristics of magnetic materials.

Recently, the authors have proposed an image processing methodology based on differential equations [3]. According to our methodology, any dynamic images so called animation can be given as a solution of the Helmholtz types of equations; we call it the image Helmholtz equation. This makes it possible to analyze an animation based on calculus and to handle an animation, consisting of several static images as frames, as continuous quantity. Further, the state transition matrix derived from our image Helmholtz equation just corresponds to the value parameterizing the physical systems. Thereby, our methodology is capable of extracting the characteristics of system from visualized information.

In this paper, we apply our methodology to the distinct magnetized domain images of a grain-oriented electrical steel observed by scanning electron microscope (SEM). It is demonstrated that solving for our image Helmholtz equations generates any magnetized state of domain images as well as continuous magnetization curves. Moreover, the iron loss generation processes are visualized by the state transition matrices derived from a series of distinct domain images.

2. Dynamic Image Representation

2.1 Governing Equation of Dynamic Images

To analyze an image visualizing physical dynamics, a representation by Helmholtz equation is regarded as an image governing equation. The key idea is that Helmholtz types of equations govern many of the physical dynamic systems. Assuming an image to be described in terms of a scalar field U, any dynamic images can be given as a solution of the Helmholtz equation [3]:

$$\nabla^2 U + \varepsilon \frac{\partial}{\partial \alpha} U = -\sigma \quad , \tag{1}$$

where ε, α and σ denote the moving speed parameter, transition variable and image source density, respectively. The first and second terms on the left in (1) represent the spatial expanse and transition of image to the variable α, respectively. The first term on the left in (1) represents a static image. The image source

density σ is given by the Laplacian operation to a final image so that the final image U_{Final} is obtained as a solution of

$$\nabla^2 U_{Final} = -\sigma \quad (2)$$

This means that the governing equation of static images is the Poisson equation [4].

2.2. Solution

Modal analysis to (1) gives a general solution:

$$U(\alpha) = \exp(-\Lambda\alpha)(U_{Start} - U_{Final}) + U_{Final}, \quad (3)$$

where U_{Start} and $\exp(-\Lambda\alpha)$ are the initial image and state transition matrix, respectively. The values ε and σ in (1) are respectively reduced into the matrix Λ and final image U_{Final}. However, the matrix Λ is unknown, since the value ε in (1) is not given. Eq. (3) generates the initial image U_{Start} if $\alpha = 0$, and the final image U_{Final} when the variable α reaches to infinity. However, α never reaches infinity so that it is necessary to determine the optimal state transition matrix from the given images.

2.3. State Transition Matrix

The matrix Λ is a key to generate the dynamic image because it corresponds to the characteristic values in various engineering. In most cases, the state transition matrix is given and derived by imposing various conditions as well as by setting physical constants of the dynamic system. In such a case, it is possible to obtain the modal matrix analytically. In our case, however, we have to determine it from several images visualized images. The problem evaluating the physical system from the visualized images is one of the inverse problems.

Let $U_{\Delta\alpha}$ be the image between the initial and final images, then it is possible to determine the elements in matrix Λ by modifying (3), as given by

$$\Lambda = -\frac{1}{\Delta\alpha}\ln\left(\frac{U_{\Delta\alpha} - U_{Final}}{U_{Start} - U_{Final}}\right). \quad (4)$$

Therefore, it is possible to analytically generate the animation by substituting the matrix Λ in (4) into (3). The solution obtained by (4) satisfies the image $U_{\Delta\alpha}$ when the variable α takes $\Delta\alpha$. Eq. (4) is one of the inverse parameter evaluation strategies using digital images.

3. Magnetic Domain Motion Analysis

3.1. SEM Domain Image and Image Helmholtz Equation

Based on the image Helmholtz equation, iron loss in magnetic material is visualized as the state transition matrix. Fig. 1 shows the magnetic domain patterns of a grain oriented silicon steel sheet under the distinct magnetized states [5]. The backscattered electron observation was carried out using scanning electron microscope (SEM). Supposing a domain image shown in Fig.1 to be composed of a scalar field U as flux density, the dynamics of domains motion can be represented by the image Helmholtz equation. In magnetizing state, the domain motion is caused by applied magnetic field H, so that the transition variable α in (3) is replaced by the magnetic field intensity H. Namely, (1) and (3) are respectively rewritten by

$$\nabla^2 U + \varepsilon\frac{\partial}{\partial H}U = -\sigma, \quad (5)$$

$$U(H) = \exp(-\Lambda H)(U_{Start} - U_{Final}) + U_{Final}. \quad (6)$$

The matrix Λ is determined by given domain images. The elements in the i-th matrix Λ_i are determined from a series of distinct SEM images in much the same way as (4), i.e.,

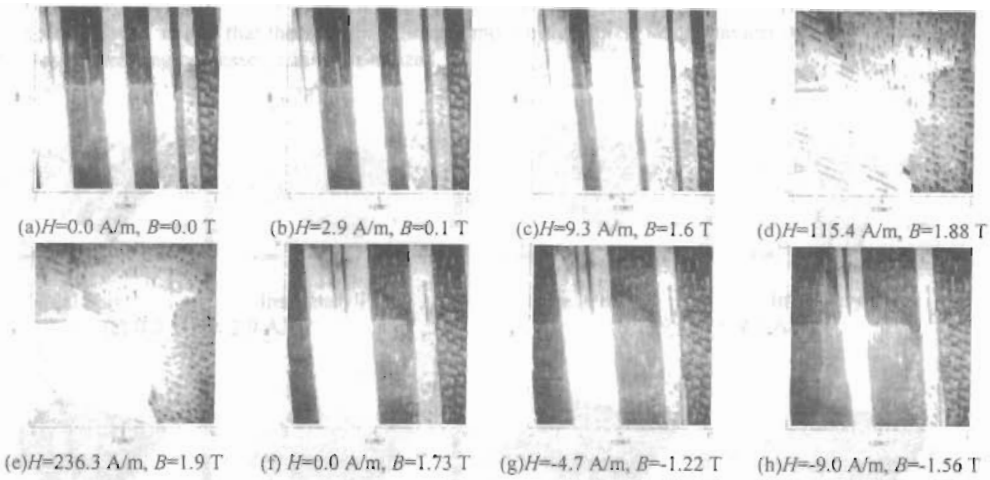

(a)H=0.0 A/m, B=0.0 T (b)H=2.9 A/m, B=0.1 T (c)H=9.3 A/m, B=1.6 T (d)H=115.4 A/m, B=1.88 T

(e)H=236.3 A/m, B=1.9 T (f) H=0.0 A/m, B=1.73 T (g)H=-4.7 A/m, B=-1.22 T (h)H=-9.0 A/m, B=-1.56 T

Fig. 1 Magnetic domain SEM images of the ORIENTCORE HI-B produced by Nippon Steel Co.(100x100 pixels, 0.1 mm/pixel)

Table 1 Measured Domain Images
H : External magnetic field intensity, B : Flux density

Image No.	H(A/m)	B(T)	Image No.	H(A/m)	B(T)
1	0.00	0.00	13	214.13	1.93
2	2.85	0.10	14	160.37	1.92
3	9.26	1.63	15	98.68	1.91
4	24.16	1.73	16	54.66	1.84
5	30.23	1.78	17	28.53	1.83
6	54.59	1.84	18	3.73	1.77
7	84.92	1.86	19	0.00	1.73
8	115.39	1.88	20	-4.60	1.73
9	160.69	1.90	21	-5.95	-0.06
10	236.32	1.92	22	-7.45	-1.43
11	324.31	1.95	23	-9.07	-1.56
12	269.64	1.95	24	-11.50	-1.62

$$\Lambda_i = -\frac{1}{\Delta H}\ln\left(\frac{U_{i+1}-U_{i+2}}{U_i-U_{i+2}}\right), \quad i=1,2,\ldots,p-2 \tag{7}$$

where the subscript i refers to a domain image number and p denotes the number of used domain images. Moreover, the images U_i and U_{i+2} correspond to the initial and final domain images, respectively. 24 domain images listed in Table 1 were used in this example, therefore, 22 matrices Λ were computed. As is well known in control theory, the elements in matrix Λ correspond to the modes of system. Extracted matrix Λ by means of (7) is capable of representing the modes of animation. In this case, the real and imaginary parts of the matrix Λ can be represented in phase and 90-degree phase different components to the applied field H. Therefore, considering Λ derived from the SEM domain images leads to *visualization of iron loss generating* parts.

3.2. Visualization of Domain Dynamics

Figure 2 shows the real and imaginary parts of the elements in the matrix Λ. The elements are displayed in accordance with these of the domain pattern in Fig.1. In the low field intensity, the real parts represent magnetic boundary displacements and magnetic domain movements (Figs. 2(a) and (b)). On the other hand, there are some values of the imaginary part in Fig. 2(b). This visualizes the force against the applied field at the grain boundary. In the high field intensity, Figs. 2(c) and (d), the magnetization process is mainly carried out by rotation of magnetization and the iron loss is caused by lancet domain appearance. Thus, based on the

matrix Λ, it has been shown that the magnetic domain motion dynamics, i.e., behaviors of magnetic domain and iron loss generating processes, can be visualized.

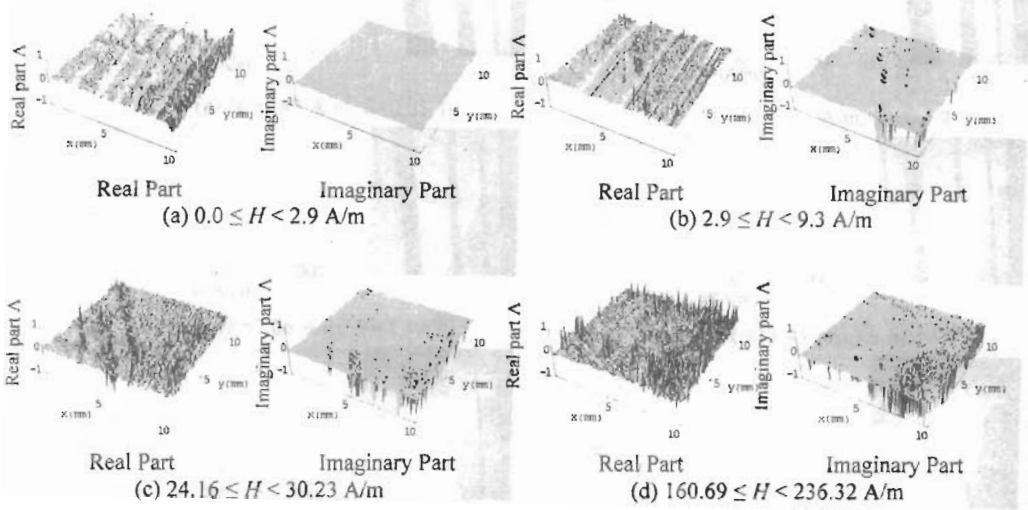

Fig. 2 State transition matrices

3.3. Domain Image Reconstruction and Magnetization Curves

Extracted matrices Λ shown in Fig.2 are characteristic value matrices to the applied field H. Eqs. (6) and (7) yield generating the domain images at arbitrary excitation. Furthermore, since the contrast of domain images represents the polarity of magnetization, then computing averaged contrast of an entire domain image gives an entire flux density. Fig.3 shows each frame of the animation generated by means of (6) and the magnetization curves. Even though the domain images represent a limited area of the specimen, the experimental result shown in Fig.4 supports our methodology.

4. Conclusions

We have proposed a method of image processing for magnetic domain images. The SEM domain images of a grain oriented silicon sheet have been examined. State transition matrices visualize the behavior of magnetic domain as well as iron loss generating parts. Moreover, a magnetization curve is reconstructed from the domain images. It is obvious that our methodology makes it possible to evaluate the magnetic material in macroscopic as well as microscopic points of view.

References

[1] L. Liorzou, B. Phelps, and D. L. Atherton, "Macroscopic models of Magnetization," IEEE Trans. Magn., vol.36, no.2, pp.418-427, 2000.
[2] A. Hubert and R. Schäfer, Magnetic Domains, Springer: Berlin, 2000.
[3] H. Endo, S. Hayano, Y. Saito, and T. L. Kunii, "A method of image processing and its application to magnetodynamic fields," Trans. IEE of Japan., vol.120-A, no.10, pp.913-918, 2000.
[4] H. Endo, S. Hayano, Y. Saito, and T. L. Kunii, "Image governing equations and its application to vector fields," Trans. IEE of Japan, vol.120-A, no.12, pp.1089-1093, 2000.
[5] T. Nozawa, T. Yamamoto, Y. Matsuo, and Y. Ohya, "Effects of scratching on losses in 3-percent Si-Fe single crystals with orientation near (110)[001]," IEEE Trans. Magn., vol.15, no.2, pp.972-981, 1979.

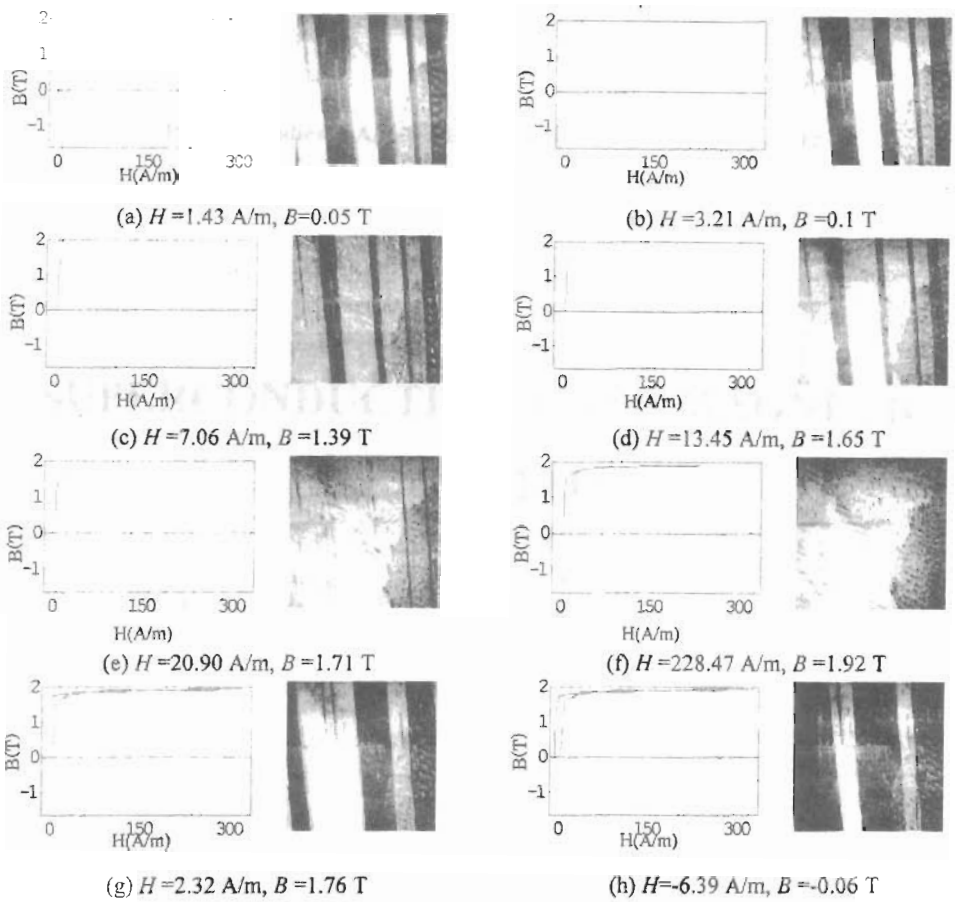

(a) H =1.43 A/m, B=0.05 T (b) H =3.21 A/m, B =0.1 T

(c) H =7.06 A/m, B =1.39 T (d) H =13.45 A/m, B =1.65 T

(e) H =20.90 A/m, B =1.71 T (f) H =228.47 A/m, B =1.92 T

(g) H =2.32 A/m, B =1.76 T (h) H=-6.39 A/m, B =-0.06 T

Fig. 3 Reconstructed domain patterns and magnetization curves

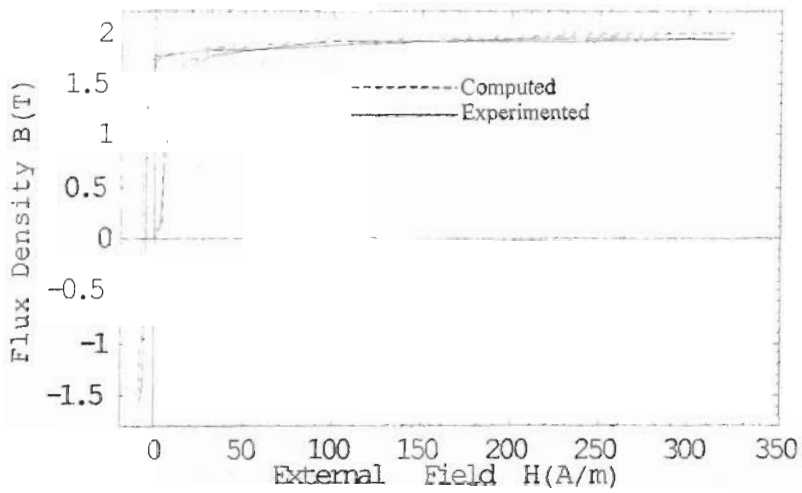

Fig. 4 Comparison computed and experimented magnetization curves